



HAL
open science

Characterization of a hyper-viscoelastic phantom mimicking biological soft tissue using an abdominal pneumatic driver with Magnetic Resonance Elastography (MRE)

Gwladys E Leclerc, Laëtitia Debernard, Félix Foucart, Ludovic Robert, Kay M Pelletier, Fabrice Charleux, Richard Ehman, Marie-Christine Ho Ba Tho, Sabine F Bensamoun

► **To cite this version:**

Gwladys E Leclerc, Laëtitia Debernard, Félix Foucart, Ludovic Robert, Kay M Pelletier, et al.. Characterization of a hyper-viscoelastic phantom mimicking biological soft tissue using an abdominal pneumatic driver with Magnetic Resonance Elastography (MRE). *Journal of Biomechanics*, 2012, 45 (6), pp.952-957. 10.1016/j.jbiomech.2012.01.017 . hal-03811582

HAL Id: hal-03811582

<https://hal.utc.fr/hal-03811582>

Submitted on 12 Oct 2022

HAL is a multi-disciplinary open access archive for the deposit and dissemination of scientific research documents, whether they are published or not. The documents may come from teaching and research institutions in France or abroad, or from public or private research centers.

L'archive ouverte pluridisciplinaire **HAL**, est destinée au dépôt et à la diffusion de documents scientifiques de niveau recherche, publiés ou non, émanant des établissements d'enseignement et de recherche français ou étrangers, des laboratoires publics ou privés.

1 **Characterization of a hyper-viscoelastic phantom mimicking biological soft**
2 **tissue using an abdominal pneumatic driver with Magnetic Resonance**

3 **Elastography (MRE)**

4 Gwladys E. Leclerc, PhD¹

5 Laetitia Debernard, PhD¹

6 Félix Foucart²

7 Ludovic Robert³

8 Kay M. Pelletier⁴

9 Fabrice Charleux, MD³

10 Richard Ehman, MD⁴

11 Marie-Christine Ho Ba Tho, PhD¹

12 Sabine F. Bensamoun, PhD¹

13
14 ¹Université de Technologie de Compiègne, UMR CNRS 6600, BioMécanique et
15 BioIngénierie, France

16
17 ²Université de Technologie de Compiègne, UMR CNRS 6253, Laboratoire Roberval de
18 Mécanique, France

19
20 ³ACRIM-Polyclinique Saint Côme, Compiègne, France

21
22 ⁴Department of Radiology, Mayo Clinic College of Medicine, Rochester, Minnesota

23
24 Original article

25 Word count: 3600 words (13 pages)

26
27 **Corresponding author**

28
29 Dr Sabine F. Bensamoun, PhD

30 Université de Technologie de Compiègne (UTC)

31 Centre de recherches de Royallieu

32 Laboratoire de BioMécanique et BioIngénierie, UMR CNRS 6600

33 Rue Personne de Roberval

34 BP 20529

35 Compiègne Cedex

36 France

37 Tel : (33) 03 44 23 43 90

38 Email: sabine.bensamoun@utc.fr

39

1 **Abstract**

2

3 The purpose of this study was to create a polymer phantom mimicking the mechanical
4 properties of soft tissues using experimental tests and rheological models.

5 Multifrequency Magnetic Resonance Elastography (MMRE) tests were performed on the
6 present phantom with a pneumatic driver to characterize the viscoelastic (μ , η) properties
7 using Voigt, Maxwell, Zener and Springpot models. To optimize the MMRE protocol, the
8 driver behavior was analyzed with a vibrometer. Moreover, the hyperelastic properties of the
9 phantom were determined using compressive tests and Mooney-Rivlin model.

10 The range of frequency to be used with the round driver was found between 60 Hz and
11 100 Hz as it exhibits one type of vibration mode for the membrane. MRE analysis revealed an
12 increase in the shear modulus with frequency reflecting the viscoelastic properties of the
13 phantom showing similar characteristic of soft tissues. Rheological results demonstrated that
14 Springpot model better revealed the viscoelastic properties ($\mu = 3.45$ kPa, $\eta = 6.17$ Pa.s) of
15 the phantom and the Mooney-Rivlin coefficients were $C_{10} = 1.09 \cdot 10^{-2}$ MPa and $C_{01} = -$
16 $8.96 \cdot 10^{-3}$ MPa corresponding to $\mu = 3.95$ kPa.

17 These studies suggest that the phantom, mimicking soft tissue, could be used for preliminary
18 MRE tests to identify the optimal parameters necessary for in vivo investigations. Further
19 developments of the phantom may allow clinicians to more accurately mimic healthy and
20 pathological soft tissues using MRE.

21

22 **Key Words:** Multifrequency Magnetic Resonance Elastography; Viscoelasticity;
23 Hyperelasticity; Phantom; Abdominal Pneumatic driver

24

1 I. INTRODUCTION

2

3 Non-invasive imaging technologies such as ultrasound-based and Magnetic
4 Resonance-based Elastography techniques have been developed, since a decade, to
5 characterize the mechanical properties of soft tissues (liver, muscle, and breast) and are
6 increasingly used in clinical practice for diagnostic purposes. In parallel to imaging methods,
7 emergence of simulating tools has required improved knowledge of the mechanical properties
8 of soft tissues (Nava et al., 2008; Marchesseau et al., 2010). The development of these
9 technologies will be enhanced by the creation of phantoms that realistically simulate the
10 mechanical properties of soft tissues. Thus, the originality of the present study was to develop
11 a phantom with mechanical properties that adequately reflect those of biological soft tissue.

12 In the literature, various phantoms have been reported, consisting of media such as
13 wirosil, agar, or bovine gels, in order to cross validate the magnetic resonance elastography
14 (MRE) technique with ultrasound technique (Oudry et al., 2009a), dynamic mechanical
15 analysis (Ringleb et al., 2005; Chen et al., 2005) and compression tests (Hamhaber et al.,
16 2003). The feasibility of the MRE technique to depict tumors was estimated with the use of
17 inclusions added to the phantom media to mimic tumors (Mariappan et al., 2009a). Moreover,
18 MRE experimental parameters such as frequency, geometry, and boundary conditions (Chen
19 et al., 2006), as well as specific MRE sequences to image dynamic organ (heart) (Kolipaka et
20 al., 2009), were previously tested on phantoms to achieve in vivo MRE tests. The mechanical
21 properties of biological tissues were further characterized with soft tissue models using in
22 vivo and in vitro experiments. Liver behavior was characterized with numerical model
23 reflected by a porous, visco-hyperelastic model using in vitro dynamic mechanical analysis
24 (Marchesseau et al., 2010). In vivo aspiration experiments have also been modeled (Nava et
25 al., 2008) using quasi-linear viscoelastic and non-linear elastic-viscoplastic models (Mazza et

1 al., 2008) to determine the mechanical properties of the liver. In addition, constitutive
2 modelling of brain tissue was done with mathematical (Miller and Chinzei, 1997) and
3 numerical (Miller, 2000) models to simulate neurosurgical procedures. The viscoelastic
4 parameter was further analyzed using multifrequency MRE technique and rheological models.
5 Thus, standard rheological models such as Maxwell, Voigt, Zener, Jeffreys and Springpot
6 models were applied to liver (Klatt et al., 2007; Asbach et al., 2008, 2010), muscle (Klatt et
7 al., 2010) and brain (Klatt et al., 2007) tissues, allowing for a better assessment of disease. In
8 addition to MRE, supersonic shear imaging was also performed to measure the viscoelastic
9 properties of muscle (Gennisson et al., 2010) and liver (Muller et al., 2009) tissue using
10 Voigt's model.

11 The purpose of this present study was to create a new generation of phantom mimicking
12 the mechanical properties of biological soft tissue using specific multifrequency magnetic
13 resonance elastography (MMRE) and compressive tests.

14

15

1 II. MATERIALS AND METHODS

3 **2.1 Phantom preparation**

4 Two homogeneous cylindrical phantoms of different sizes (Diameter: 25 cm with a
5 thickness of 5 cm and diameter: 2.6 cm with a height of 3.8 cm) were created with an
6 elasticity similar to that of muscle tissue (Bensamoun et al., 2006). The cylindrical phantoms
7 analyzed in the present study were composed of 45% softener and 55% liquid plastic
8 (LureCraft, LaGrande, USA), or plastisol, which is a suspension of PVC particles in a
9 plasticizer. The mixture was heated to 177°C, poured into cylindrical silicone molds and left
10 to cool at room temperature (23°C) until the phantoms solidified. The reproducibility of the
11 phantom process induced a variability of the elastic properties (μ) about 10%. Then, the
12 phantoms were stocked and preserved at room temperature (23°C).

14 **2.2 Abdominal driver behavior**

15 A laser doppler vibrometer (PSV 400, Polytec, France) was used to determine the
16 accurate displacement of the membrane induced by the round driver at 60 Hz. Figure 1a
17 shows the fixation of the driver placed to a distance of 74.3 cm from the vibrometer. Tests
18 were performed from 0 Hz to 300 Hz to observe the magnitude of the membrane's
19 deformation. A laser scaled the entire membrane with an angular resolution of approximately
20 0.002°, providing a mesh of the membrane composed of 171 nodes (Fig. 1a). The maximal
21 displacement of membrane (D) was recorded for a frequency range of 60 Hz to 100 Hz,
22 representing values typically applied to biological soft tissue (liver, muscle) using MRE.

2.3 Multifrequency Magnetic Resonance Elastography (MMRE) tests

MMRE experiments were performed on the larger phantom inside a 1.5T (General Electric Signa HDx) MRI machine. The phantom was placed inside a head coil (Fig. 2a), resting on a round pneumatic driver, connected to a large active loudspeaker. The driver generates shear waves through the phantom at three frequencies (60 Hz, 70 Hz, 80 Hz), representing values typically applied to biological soft tissue (liver, muscle) using MRE. This driver is currently used for studying the liver (Yin et al., 2007), and consists of a thin flexible membrane (10-20 μm) made of polycarbonate enclosed by rigid walls, with a resonance frequency of 30 Hz. To avoid extraneous motion of the phantom during the MRE test, a support cushion was placed under the phantom.

MRE phase images (Fig. 2b) were collected using a motion sensitizing gradient echo sequence, a flip angle of 45° , a 30 x 30 cm field of view and a 256 x 64 acquisition matrix. Phase images composed of four offsets were recorded for each different frequency, with a TE corresponding to the minimum echo time allowing for motion encoding, and a TR equal to 50 ms, 43 ms and 38 ms at 60 Hz, 70 Hz and 80 Hz, respectively. Multifrequency MR Elastography tests allow for the characterization of the elastic properties of the phantom for each frequency. Moreover, the variation of the wavelengths as a function of the frequency will allow an analysis of the viscoelastic behavior. Thus, elastic properties were characterized, assuming that the media was linear elastic, isotropic and homogeneous, leading to the shear modulus (μ) using the following equation: $\mu = \rho (f\lambda)^2$, where ρ is the density of the phantom (1000 kg/m^3), f is the frequency (Hz) and λ is the shear wavelength (m). The wavelengths (Fig. 2c) were measured from the phase images (Fig. 2b) with a 1D profile drawn along the radial direction of the propagation of the shear wave and located in the same area for each phase image. Then, the shear modulus was calculated for each frequency. From the phase images, the corresponding cartography of the shear modulus (Fig. 2d) was generated using the

1 local frequency estimate (LFE) algorithm (Manduca et al., 2001), providing a spatial
2 distribution of the elastic properties.

3 The larger phantom underwent the first MRE test (test #1) one month after its
4 development, and a follow up of the phantom behavior was done every month with
5 reproducibility tests. Tests #2 and #3 corresponding to MRE tests performed at 5 and 11
6 months will be presented.

7

8 **2.4 Viscoelastic modelling**

9 The viscoelastic behavior being represented by an elastic (shear modulus: μ) and a
10 viscous (the viscosity: η) components, four different rheological models (Voigt, Maxwell,
11 Zener and Springpot) were used. These models are composed of springs and dashpots (Klatt
12 et al., 2007), reflecting a complex shear modulus (G^* , kPa) related to shear stiffness (μ , kPa),
13 viscosity (η , Pa.s), and excitation pulsation (ω , Hz). To quantify the rheological coefficients
14 (μ , η), an identification method was performed using a mean squared analysis with Matlab
15 R2008b software (The Matworks, Inc., Natick, MA), based on a cost function composed of
16 experimental velocities from the multifrequency MRE tests and theoretical velocities from
17 Helmholtz equation (Bourbie et al., 1986) applied to rheological models.

18

19 **2.5 Mechanical tests**

20 Compression tests were performed on the smaller cylindrical phantom with a texture analyzer
21 machine (Fig. 3a) (XT Plus, Stable Micro Systems, England). The samples were placed
22 between a load cell and a heavy duty platform while a compressive force until 3 N was
23 applied with a velocity of 0.5 mm/s. Then, the displacement (mm) as a function of the force
24 (N) was recorded and normalized by the sample surface in order to obtain the representative

1 stress-strain curve of the behavior of the phantom (Fig. 3b). The mechanical test was repeated
 2 twice on the sample.

3

4 **2.6 Hyperelastic characterization**

5 As expected by the composition of the phantom, a non-linear curve reflecting the
 6 phantom behavior was obtained. The stress-strain curve was computed with ABAQUS 6-9.1
 7 Standard (Simulia Dassault Systems) in order to further characterize the non-linear properties
 8 of the phantom. As it is well known that non-linear behavior is represented by a hyperelastic
 9 model, the Mooney-Rivlin model was used, assuming that the material was isotropic and
 10 incompressible. This model is based on the strain energy function with a polynomial
 11 development of first order. In case of uniaxial compression, the relationship between
 12 engineering stress and strain is defined by the following equation (Miller and Chinzei, 1997):

$$13 \quad \sigma = 2 \cdot \left(\lambda^2 - \frac{1}{\lambda} \right) \cdot \left(C_{10} + \frac{C_{01}}{\lambda} \right) \text{ with } \lambda = \frac{L}{L_0}$$

14 where σ is the engineering stress (MPa), λ is the deformation, L is the length of phantom
 15 during the mechanical test (mm) and L_0 the initial length of sample (3.8 cm). The coefficients
 16 C_{10} and C_{01} are the Mooney-Rivlin's parameters (MPa). In addition, the shear stiffness (μ ,
 17 MPa) was also calculated using the following equation (Miller and Chinzei, 1997):

$$18 \quad \mu = 2 \cdot (C_{10} + C_{01})$$

19

20

1 III. RESULTS

2

3 **3.1 Characterization of the elastic properties using MMRE tests**

4 Phase images obtained as a function of time (1, 5 and 11 months) and frequency (60 Hz,
5 70 Hz and 80 Hz) represent the propagation of shear waves inside the larger phantom. A more
6 uniform shape of the wave was observed at 60 Hz (Fig. 4a, d and g) as compared to 80 Hz
7 (Fig. 4c, f, and i), where gaps begin to occur. This result reveals that 60 Hz is the optimal
8 frequency to use for the characterization of the elastic properties of the present phantom.
9 Moreover, it can be noted that the phantom exhibited a range of shear modulus between 3.3
10 and 4.3 kPa, whatever the frequency and the time are.

11 Test #1 showed a quasi-elastic behavior of the phantom, reflected by a homogeneous
12 spatial distribution of stiffness (Fig. 4a) and by a slight increase of the shear modulus
13 (0.10 kPa) as a function of the frequency. However, test #2 and #3 revealed a higher increase
14 in the shear modulus measured from 60 Hz to 80 Hz ($\Delta\mu_{\text{test2}} = 0.18$ kPa, $\Delta\mu_{\text{test3}} = 0.19$ kPa),
15 indicating an increase of the viscoelastic behavior with time. In addition, for each frequency,
16 the cartographies of stiffness showed a slight stiffening of the phantom media from 1 to 11
17 months, reflected by an increase in the elastic properties of $\Delta\mu_{60\text{Hz}} = 0.82$ kPa,
18 $\Delta\mu_{70\text{Hz}} = 0.80$ kPa, $\Delta\mu_{80\text{Hz}} = 0.91$ kPa. The reproducibility tests showed a variation of the
19 shear modulus measurement about 1.7%.

20

21 **3.2 Characterization of abdominal driver behavior**

22 Figure 5 shows the eigenfrequencies of the membrane characterized from 0 Hz to
23 300 Hz, where the resonant frequency of the loudspeaker was observed to be around 30 Hz.
24 Between 60 Hz and 100 Hz, the flexible membrane exhibited only one type of vibration
25 mode, represented by a unique antinode. After 100 Hz, the deformation of the membrane

1 contained different shapes composed of another eigenmode, representing a non-uniform
2 deformation of the membrane. For instance, at 110 Hz, two distinct antinodes were identified
3 indicating that different areas of the membrane are vibrated at this frequency. Thus, the range
4 of frequencies to be used with this round driver is between 60 Hz and 100 Hz.

5 The results showed a higher magnitude of displacement for 60 Hz and 80 Hz
6 ($D_{60\text{Hz}} = 39.2 \mu\text{m}$, $D_{80\text{Hz}} = 40.2 \mu\text{m}$) compared to 70 Hz ($D_{70\text{Hz}} = 31.5 \mu\text{m}$), 90 Hz
7 ($D_{90\text{Hz}} = 31.0 \mu\text{m}$) and 100 Hz ($D_{100\text{Hz}} = 25.9 \mu\text{m}$).

8

9 **3.3 Characterization of the viscoelastic and hyperelastic properties**

10 Table 1 shows the rheological parameters (shear modulus: μ and viscosity: η) at 1, 5 and
11 11 months obtained using the four models. The comparison of the elastic properties obtained
12 with MMRE and rheological models showed similar values of the shear modulus as a function
13 of time. The viscoelastic parameters for test #1 revealed lower viscosities (from 1.18 to
14 6.17 Pa.s) for the solid models (Voigt, Zener and Springpot) compared to the fluid model
15 (Maxwell) which showed a higher viscosity (18.09 Pa.s) due to its property to reflect the
16 viscous component. This result attested that the identification method is capable of
17 differentiating solid and fluid behaviors. All models demonstrated a slight increase of the
18 viscoelastic parameters over time. It can be noted that the Springpot model revealed the
19 highest increase in the viscoelastic parameters compared to the other models. Hyperelastic
20 properties were determined from the nonlinear stress-strain curves (Fig. 3b) that were
21 obtained with the compressive tests, allowing for the measurement of the Mooney-Rivlin
22 coefficients ($C_{10} = 1.09 \cdot 10^{-2} \text{ MPa}$ and $C_{01} = -8.96 \cdot 10^{-3} \text{ MPa}$). The corresponding shear
23 stiffness was 3.95 kPa, which is in the same range as the previous elastic properties obtained
24 with the multifrequency MRE tests.

25

1 IV. DISCUSSION

2

3 Magnetic resonance elastography (MRE) has been extensively developed to
4 characterize the elastic properties of biological soft tissue such as liver (Rouvière et al., 2006)
5 or muscle (Bensamoun et al., 2008). Thus, the purpose of this study was to demonstrate that
6 the present phantom could be used for future MRE tests to mimic the mechanical properties of
7 healthy human soft tissue. In the literature, different types of phantoms (wirosil, agar, bovine
8 gel) were also developed to validate the MRE technique before performing in vivo tests.
9 Indeed, elastic properties of agarose gel were characterized with MRE, in a range of 4 kPa to
10 130 kPa for different concentrations and excitation frequencies (from 100 to 400 Hz) (Ringleb
11 et al., 2005, Chen et al., 2005, and Hamhaber et al., 2003). Another kind of phantom in a
12 range of 1 kPa to 8 kPa, composed of copolymer-in-oil and B-gel, was analyzed with MRE
13 tests using the same mechanical frequency (60 Hz) as the present study (Oudry et al., 2009a).

14 Elastic properties of healthy skeletal muscle at rest are represented by a shear modulus
15 in a range of 2-4 kPa (Bensamoun et al., 2006), which is similar to the present phantom
16 behavior. In the literature, the viscoelastic properties of skeletal muscle and liver tissues were
17 quantified with Voigt and Zener's models (Klatt et al., 2007; Gennisson et al., 2010) and the
18 use of these models to the present phantom demonstrated a quasi-constant viscosity
19 (maximum of increase about 1 Pa.s at 5 months and 2 Pa.s at 11 months) as a function of
20 time. To our knowledge, the present phantom is the first one to reflect both the elastic and
21 viscoelastic properties of healthy biological tissue when testing with the MRE technique.
22 Moreover, this new generation of phantom has the advantage to keep approximately the same
23 viscoelastic properties over time unlike organic phantoms (agarose or bovine gel) which are
24 unstable (Oudry et al., 2009b).

1 To better characterize the viscoelastic behavior of the phantom, a fractionary solid
2 model (Springpot) was used, composed of a third parameter (coefficient α) allowing
3 acquisition of information about the viscous component of the model. Indeed, when α tends to
4 1, the model is purely viscous represented by only one dashpot, and when α tends to 0, the
5 model becomes purely solid represented by only one spring. The Springpot model
6 demonstrated the highest increase in viscosity, which was also observed through MRE tests.
7 Therefore, it was concluded that this model is the most adapted rheological model to quantify
8 the viscoelastic properties of the phantom. Furthermore, the viscosity obtained in this present
9 study at one month (6.17 Pa.s) was in agreement with the viscosity fixed for the liver tissue
10 (7.30 Pa.s) by Asbach et al. (2010), as well as the viscosities fixed for quadriceps muscles (1-
11 10 Pa.s) by Klatt et al. (2010) using MRE. In addition to the viscoelastic parameter, the elastic
12 properties measured with the same Springpot model at one month (3.45 kPa) was similar to
13 the one measured using MRE ($\mu_{60\text{Hz}} = 3.34$ kPa, $\mu_{80\text{Hz}} = 3.44$ kPa). The Springpot model
14 seems to be more adapted to representing the mechanical properties (μ , η) of the biological
15 soft tissues, and the present study confirmed the feasibility of the phantom to reflect the
16 elastic (μ) and viscoelastic (η) properties of soft tissues.

17 During the last decade, drivers were optimized with new designs such as the
18 assemblage of mechanical drivers for heart tissue (Mariappan et al., 2009b), a pneumatic tube
19 for muscle tissue (Bensamoun et al., 2006) or a round pneumatic driver for the liver (Yin et
20 al., 2007). In addition to the design, drivers were also further developed to improve the quality
21 of shear wave propagation by sending longitudinal vibrations, (Yin et al., 2008) leading to an
22 improvement in the measurement of elastic properties measurement. However, none of the
23 previous studies have analyzed the mechanical behavior of the used driver. The present study
24 showed the importance of this characterization to optimize the range of frequency to apply to
25 each driver. We demonstrated that the range of frequency to be used with the round driver

1 was between 60 Hz and 100 Hz as it exhibits one type of vibration mode for the membrane.
2 However, MRE tests demonstrate a better propagation at 60 Hz, explaining why in the
3 literature in vivo stiffness of biological soft tissues was characterized at 60 Hz using MRE
4 with the same round pneumatic driver.

5 Magnetic Resonance Elastography is a clinical tool already implemented in the United
6 States and Europe for liver tissue, and many other tissues as well as organs are under
7 investigation with this non-invasive technique. The present study demonstrated the necessity
8 to characterize the driver properties in order to set up specific MRE test's protocols. This new
9 phantom, mimicking the mechanical properties of biological soft tissue, could be the first step
10 to define optimal MRE parameters before in vivo investigations. It will be of interest to
11 further develop the phantom behavior to more accurately mimic healthy and pathological soft
12 tissues using MRE.

13

1 **ACKNOWLEDGEMENTS**

2 This work was supported by the Picardie Region and NIH grant EB001981. We thank Pierre
3 Feissel, assistant professor, for the use of the laser Doppler vibrometer.

4

5

1 **References**

- 2 Asbach, P., Klatt, D., Hamhaber, U., Braun, J., Somasundaram, R., Hamm, B., Sack, I.,
3 2008. Assessment of liver viscoelasticity using multifrequency MR elastography. *Magnetic*
4 *Resonance in Medicine* 60(2), 373-379.
- 5 Asbach, P., Klatt, D., Schlosser, B., Biermer, M., Muehe, A., Rieger, A., Loddenkemper,
6 C., Somasundaram, R., Berg, T., Hamm, B., Braun, J., Sack, I., 2010. Viscoelasticity-based
7 staging of hepatic fibrosis with multifrequency MR elastography. *Radiology* 257(1), 80-86.
- 8 Bensamoun, S. F., Ringleb, S. I., Littrell, L., Chen, Q., Brennan, M., Ehman, R. L., 2006.
9 Determination of thigh muscle stiffness using magnetic resonance elastography. *Journal of*
10 *Magnetic Resonance Imaging* 23, 242-247.
- 11 Bensamoun, S. F., Glaser, K. J., Ringleb, S. I., Chen, Q., Ehman, R. L., 2008. Rapid
12 magnetic resonance elastography of muscle using one dimensional projection. *Journal of*
13 *Magnetic Resonance Imaging* 27, 1083-1088.
- 14 Bourbié, T., Coussy, O., Zinszner, B., 1986. *Acoustique des milieux poreux*. Editions
15 *Technip*, pp. 99-138.
- 16 Bro-Nielsen, M. (1998). Finite element modelling in surgery simulation. In *Proceedings of*
17 *the IEEE* 86(3), 490-503.
- 18 Chen, Q., Ringleb, S. I., Hulshizer, T., An, K-N., 2005. Identification of the testing
19 parameters in high frequency dynamic shear measurement on agarose gels. *Journal of*
20 *Biomechanics* 38(4), 959-963.
- 21 Chen, Q., Ringleb, S. I., Manduca, A., Ehman, R. L., An, K-N., 2006. Differential effects
22 of pre-tension on shear wave propagation in elastic media with different boundary conditions
23 as measured by magnetic resonance elastography and finite element modelling. *Journal of*
24 *Biomechanics* 39(8), 1428-1434.

- 1 Gennisson, J. L., Deffieux, T., Mace, E., Montaldo, G., Fink, M., Tanter, M. L., 2010.
2 Viscoelastic and Anisotropic Mechanical Properties of in vivo Muscle Tissue Assessed by
3 Supersonic Shear Imaging. *Ultrasound in Medicine & Biology* 36(5), 789-801.
- 4 Hamhaber, U., Grieshaber, F. A., Nagel, J. H., Klose, U., 2003. Comparison of quantitative
5 shear wave MR-elastography with mechanical compression tests. *Magnetic Resonance in*
6 *Medicine* 49(1), 71-77.
- 7 Klatt, D., Hamhaber, U., Asbach, P., Braun, J., Sack, I., 2007. Noninvasive assessment of
8 the rheological behavior of human organs using multifrequency MR elastography: a study of
9 brain and liver viscoelasticity. *Physics in Medicine and Biology* 52, 7281-7294.
- 10 Klatt, D., Papazoglou, S., Braun, J., Sack, I., 2010. Viscoelasticity-based MR elastography
11 of skeletal muscle. *Physics in Medicine and Biology* 55, 6445-6459.
- 12 Kolipaka, A., McGee, K. P., Araoz, P. A., Glaser, K. J., Manduca, A., Ehman, R. L., 2009.
13 Evaluation of a rapid, multiphase MRE sequence in a heart-simulating phantom. *Magnetic*
14 *Resonance in Medicine* 62(3), 691-698.
- 15 Manduca, A., Oliphant, T.E., Dresner, M. A., Mahowald, J. L., Kruse, S. A., 2001.
16 Magnetic resonance elastography: non-invasive mapping of tissue elasticity. *Medical Image*
17 *Analysis* 5, 237-254.
- 18 Marchesseau, S., Heimann, T., Chatelin, S., Willinger, R., 2010. Multiplicative jacobian
19 energy decomposition method for fast porous visco-hyperelastic soft tissue model. *Lecture*
20 *Notes in Computer Science* 6361, 235-242.
- 21 Mariappan, Y. K., Glaser, K. J., Manduca, A., Romano, A. J., Venkatesh, S. K., Yin, M.,
22 Ehman, R. L., 2009a. High-frequency mode conversion technique for stiff lesion detection
23 with magnetic resonance elastography (MRE). *Magnetic Resonance in Medicine* 62(6), 1457-
24 1465.

- 1 Mariappan, Y. K., Rossman, P. J., Glaser, K. J., Manduca, A., Ehman, R. L., 2009b.
2 Magnetic resonance elastography with a phased-array acoustic driver system. *Magnetic*
3 *Resonance in Medicine* 61(3), 678-685.
- 4 Mazza, E., Grau, P., Hollenstein, M., Bajka, M., 2008. Constitutive Modelling of Human
5 Liver Based on in Vivo Measurements. In *Proceedings of the 11th International Conference*
6 *on Medical Image Computing and Computer-Assisted Intervention, Part II*, Springer-Verlag.
- 7 Miller, K., 2000. Constitutive modelling of abdominal organs. *Journal of Biomechanics* 33,
8 367-373.
- 9 Miller, K., Chinzei, K., 1997. Constitutive modelling of brain tissue experiment and
10 theory. *Journal of Biomechanics* 30, 1115-1121.
- 11 Muller, M., Gennisson, J-L., Deffieux, T., Tanter, M., Fink, M., 2009. Quantitative
12 Viscoelasticity Mapping of Human Liver Using Supersonic Shear Imaging: Preliminary In
13 Vivo Feasibility Study. *Ultrasound in Medicine & Biology* 35(2), 219-229.
- 14 Nava, A., Mazza, E., Furrer, M., Villiger, P., Reinhart, W. H., 2008. In vivo mechanical
15 characterization of human liver. *Medical Image Analysis* 12(2), 203-216.
- 16 Oudry, J., Chen, J., Glaser, K. J., Miette, V., Sandrin, L., Ehman, R. L., 2009a. Cross-
17 validation of magnetic resonance elastography and ultrasound-based transient elastography: A
18 preliminary phantom study. *Journal of Magnetic Resonance Imaging* 30(5), 1145-1150.
- 19 Oudry, J., Bastard, C., Miette, V., Willinger, R., Sandrin, L., 2009b. Copolymer-in-oil
20 phantom materials for elastography. *Ultrasound in Medicine & Biology* 35(7), 1185-1197.
- 21 Ringleb, S. I., Chen, Q., Lake, D. S., Manduca, A., Ehman, R. L., An, K-N., 2005.
22 Quantitative shear wave magnetic resonance elastography: comparison to a dynamic shear
23 material test. *Magnetic Resonance in Medicine* 53(5), 1197-1201.
- 24 Rouvière, O., Yin, M., Dresner, M A., Rossman, P. J., Burgart, L. J., Fidler, J. L., Ehman,
25 R. L., 2006. MR Elastography of the liver: preliminary results. *Radiology* 240(2), 440-448.

1 Yin, M., Talwalkar, J. A., Glaser, K. J., Manduca, A., Grimm, R. C., Rossman, P. J.,
2 Fidler, J. L., Ehman, R. L., 2007. Assessment of hepatic fibrosis with magnetic resonance
3 elastography. *Clinical Gastroenterology and Hepatology* 5(10), 1207-1213.

4 Yin, M., Rouvière, O., Glaser, K. J., Ehman, R. L., 2008. Diffraction-biased shear wave
5 fields generated with longitudinal magnetic resonance elastography drivers. *Magnetic*
6 *resonance imaging* 26(6), 770-780.

7

1 **Table**

2

| | Elastic case | Voigt | Maxwell | Zener | Springpot |
|-----------------------------------|--|--|---|--|---|
| Test #1 1month | $\mu_{60\text{Hz}} = 3.34 \text{ kPa}$ $\mu_{70\text{Hz}} = 3.41 \text{ kPa}$ $\mu_{80\text{Hz}} = 3.44 \text{ kPa}$ | $\mu = 3.24 \text{ kPa}$ $\eta = 1.84 \text{ Pa.s}$ | $\mu = 4.48 \text{ kPa}$ $\eta = 18.09 \text{ Pa.s}$ | $\mu_1 = 3.23 \text{ kPa}$ $\mu_2 = 2.44 \text{ kPa}$ $\eta = 1.18 \text{ Pa.s}$ | $\mu = 3.45 \text{ kPa}$ $\alpha = 0.088$ $\eta = 6.17 \text{ Pa.s}$ |
| Test #2 5months | $\mu_{60\text{Hz}} = 4.09 \text{ kPa}$ $\mu_{70\text{Hz}} = 4.14 \text{ kPa}$ $\mu_{80\text{Hz}} = 4.27 \text{ kPa}$ | $\mu = 3.85 \text{ kPa}$ $\eta = 2.84 \text{ Pa.s}$ | $\mu = 4.48 \text{ kPa}$ $\eta = 17.79 \text{ Pa.s}$ | $\mu_1 = 3.82 \text{ kPa}$ $\mu_2 = 3.38 \text{ kPa}$ $\eta = 1.97 \text{ Pa.s}$ | $\mu = 3.97 \text{ kPa}$ $\alpha = 0.138$ $\eta = 11.57 \text{ Pa.s}$ |
| Test #3 11months | $\mu_{60\text{Hz}} = 4.16 \text{ kPa}$ $\mu_{70\text{Hz}} = 4.21 \text{ kPa}$ $\mu_{80\text{Hz}} = 4.35 \text{ kPa}$ | $\mu = 3.89 \text{ kPa}$ $\eta = 4.62 \text{ Pa.s}$ | $\mu = 4.62 \text{ kPa}$ $\eta = 17.02 \text{ Pa.s}$ | $\mu_1 = 3.88 \text{ kPa}$ $\mu_2 = 9.98 \text{ kPa}$ $\eta = 2.56 \text{ Pa.s}$ | $\mu = 4.17 \text{ kPa}$ $\alpha = 0.156$ $\eta = 9.60 \text{ Pa.s}$ |

3

4 Table 1: Shear modulus (μ) obtained with the multifrequency MRE tests as well as
5 rheological models allowing also for the characterization of the viscosity (η) with its
6 proportional coefficient (α) for the phantom.

7

8

9

1 **Figure legends**

2

3 Fig. 1. Characterization of the membrane deformation, from 0 to 300 Hz, with a laser doppler
4 vibrometer. Mesh of the membrane composed of 171 nodes where each displacement was
5 acquired (A). Visualization of the entire shape of the membrane at 60Hz where the maximal
6 displacement (39.2 μ m) was measured (B).

7

8 Fig. 2. Experimental setup for Magnetic Resonance Elastography (MRE) tests performed at
9 60 Hz on the phantom (A). Acquisition of the phase image (B), placement of the profile (C)
10 and elastograms (D) obtained with LFE algorithm.

11

12 Fig. 3. Compression test performed on the phantom with a texture analyzer (A) with the non-
13 linear stress-strain recorded curve (B).

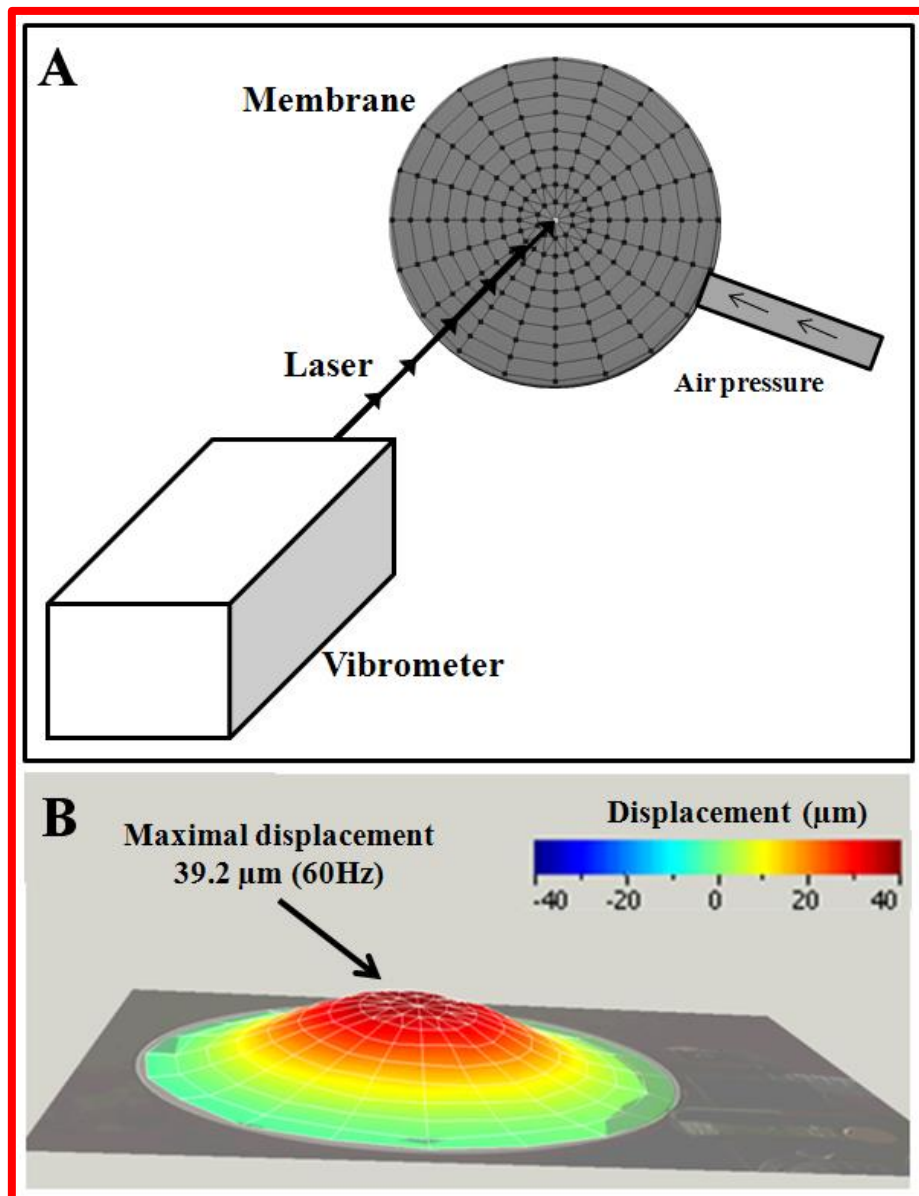
14

15 Fig. 4. Representation of the phase images and the corresponding cartography of shear
16 modulus obtained through MRE tests performed at 1 (test #1), 5 (test #2) and 11 (test #3)
17 months at three different frequencies 60 Hz, 70 Hz and 80 Hz.

18

19 Fig. 5. Illustration of the entire membrane displacement obtained with a laser doppler
20 vibrometer from 0 to 300 Hz associated to the frequency response spectrum. The round
21 pneumatic driver showed the same vibration mode for the membrane only between 60 Hz and
22 100 Hz.

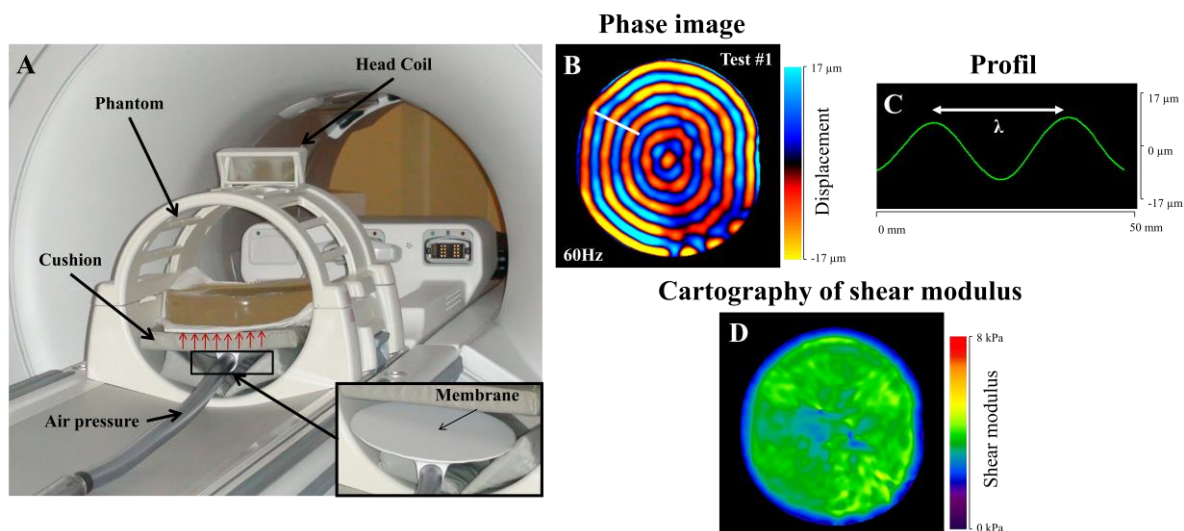
23

1 **Figures**

2

3 Fig. 1. Characterization of the membrane deformation, from 0 to 300 Hz, with a laser doppler
 4 vibrometer. Mesh of the membrane composed of 171 nodes where each displacement was
 5 acquired (A). Visualization of the entire shape of the membrane at 60Hz where the maximal
 6 displacement (39.2 μm) was measured (B).

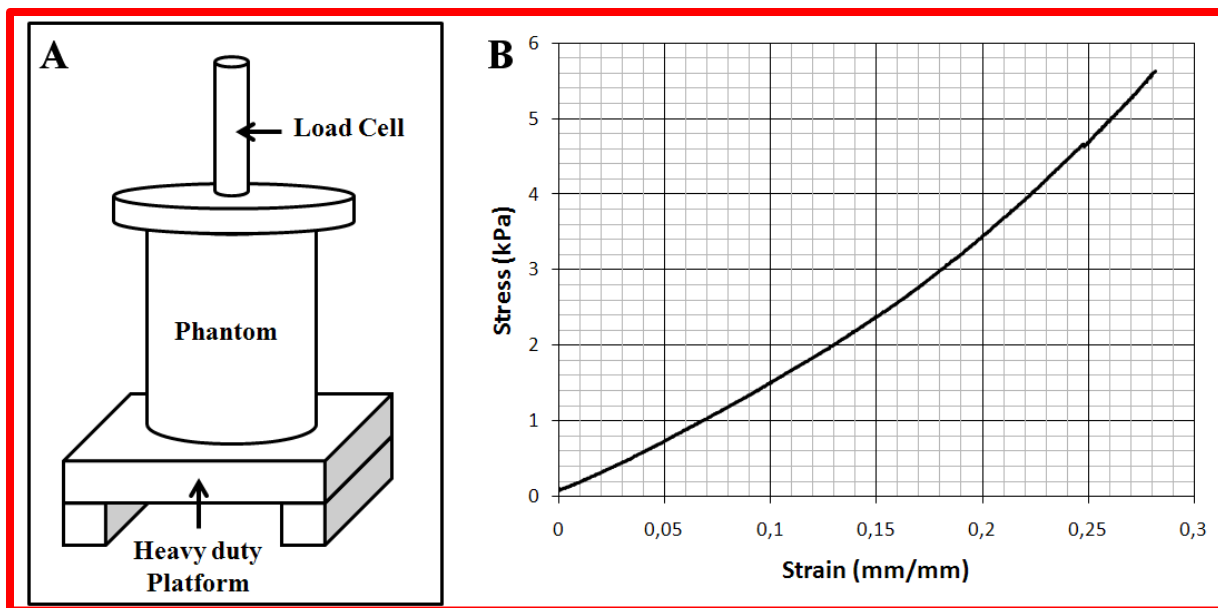
7



1

2 Fig. 2. Experimental setup for Magnetic Resonance Elastography (MRE) tests performed at
 3 60 Hz on the phantom (A). Acquisition of the phase image (B), placement of the profile (C)
 4 and elastograms (D) obtained with LFE algorithm.

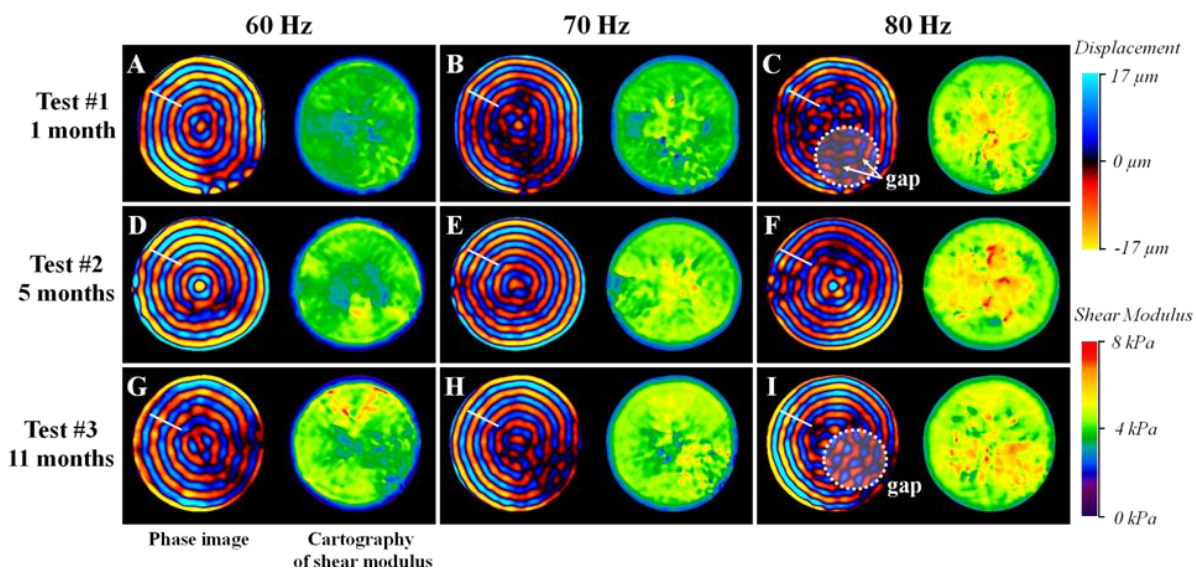
5



1

2 Fig. 3. Compression test performed on the phantom with a texture analyzer (A) with the non-
3 linear stress-strain recorded curve (B).

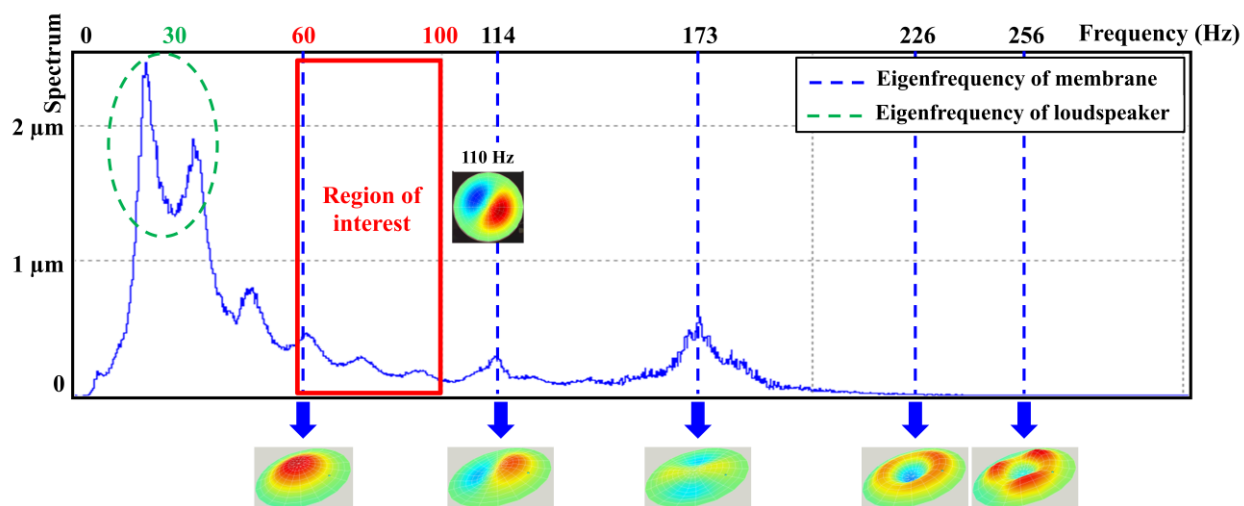
4



1

2 Fig. 4. Representation of the phase images and the corresponding cartography of shear
 3 modulus obtained through MRE tests performed at 1 (test #1), 5 (test #2) and 11 (test #3)
 4 months at three different frequencies 60 Hz, 70 Hz and 80 Hz.

5



1

2 Fig. 5. Illustration of the entire membrane displacement obtained with a laser doppler
 3 vibrometer from 0 to 300 Hz associated to the frequency response spectrum. The round
 4 pneumatic driver showed the same vibration mode for the membrane only between 60 Hz and
 5 100 Hz.

6